Open Access and Peer Reviewed Journal ISSN 2395-1303 https://www.ijetjournal.org/

RESEARCH ARTICLE OPEN ACCESS

Fuzzy Logic-Controlled Nine-Level Inverter for Solar PV Integrated Grid-Connected Bidirectional EV charging

Mekala Jahnavi[1]

PG Student

Department of EEE

SVUCE, Sri Venkateswara University

Tirupati, India-517502

mekalajahnavi1@gmail.com

Yerramsetty Pavani[2]

Academic Consultant

Department of EEE

SVUCE, Sri Venkateswara University

Tirupati, India-517502

pavani716@gmail.com

Abstract — This paper presents a fuzzy logic controller (FLC) for a grid-connected Nine-level inverter integrating a Solar photovoltaic (PV) source and a bidirectional electric vehicle (EV) battery. Conventional PI controllers perform well under fixed operating conditions, but their performance may be affected by rapid changes in solar irradiance, nonlinear loads, and EV battery charging or discharging conditions. To overcome these limitations, a fuzzy logic controller is used to provide better control under changing and discharging operating conditions without depending entirely on an accurate mathematical model. The suggested system employs fuzzy control for maximum power point tracking (MPPT), battery integration, and inverter management, with nine-level inverter functioning as an active filter to attenuate harmonics produced by non-linear loads. The system performance was evaluated based on THD, settling time, overshoot, and response to variations in irradiance and load. Compared with conventional PI control, the simulation results show that the proposed controller reduces the grid current THD to 1.14%, providing a faster MPPT response, lower current distortion, smoother battery charging and discharging and providing lower harmonic distortions, and increase in power quality. The integrated PV, nine-level inverter, and EV battery system can therefore be considered for grid-connected renewable energy systems, microgrids, smart grid applications, and V2G or G2V operations.

Keywords — Fuzzy Logic controller (FLC), Grid to Vehicle (G2V), Proportional Integral (PI)controller, Total harmonic distortion (THD), vehicle to grid(V2G).

I. INTRODUCTION

Increase in use of solar photovoltaic (PV) energy for electric vehicle (EV) charging requires a power-conversion system that can handle changes in PV generation, battery demand, grid power, and nonlinear loads [9]. Recent research has explored nine-level multilevel inverters for PV applications, multilevel converters for EV and battery systems and PV inverters with shunt active-filter operation [2], [3], [8], [12]. However, these functions have mostly been considered in different system configurations, leaving scope for an integrated PV–EV system with a suitable control method.

In this work, a grid-connected nine-level inverter is developed by integrating a solar PV source, EV lithium-ion battery, utility grid, nonlinear load, and filter. A TOSSI-based fuzzy logic controller (FLC) is used to control the inverter, while a bidirectional DC-DC converter enables battery charging/ discharging. The inverter also compensates for harmonics produced by the nonlinear load. The simulation results for different PV and battery operating conditions show a reduction in grid-current THD from 6.64% to 1.14% when the FLC and filter are used.

The rest of the paper presents the proposed system, control method, simulation results, and performance analysis, followed by the conclusion.

II. LITERATURE REVIEW

The emerging use of solar photovoltaics (PV) in the integration of electric vehicles (EVs) with EV charging poses the need for converters capable of coping with the variability in solar power generation, battery requirements and grid conditions. Solar power varies depending on the level of solar irradiance and temperature. On the other hand, an EV battery needs different power depending on whether it is being charged or is discharging the stored energy back to the grid [9].

Predictive control for PV-integrated EV chargers was discussed in [1], whereas a review on converters used in grid-connected PV- powered EVs with bidirectional power flow was done in [9].

Multilevel inverters (MLIs) are considered in renewable energy due to the fact that MLIs produce output voltage via several steps and therefore reduce the magnitude of voltage steps [4], [14]. A new multilevel inverter architecture was proposed for a grid-connected PV system in [3], whereas the performance of an asymmetrical reduced-switch multilevel inverter in grid-connected PV operation was discussed in [2]. The Reduced-switch MLI architecture was further reviewed in [4]. Sathik et al. experimentally studied a self-voltage-balanced nine-level ANPC inverter for PV applications [6]. The operation of a PV cascaded H-bridge inverter in varying meteorological conditions was analyzed in [5]. Moreover, the power quality characteristics of grid-connected cascaded H-bridge nine-level inverters were analyzed in [8]. Also, Al-Samawi and Trabelsi have developed a nine-level cascaded inverter topology using a reduced number of switches in PV applications [12]. The above references give some basis to select the multilevel inverter topologies for use in PV-fed grid-connected systems.

Control plays an important role in sustaining the performance of PV conversion systems during varying operational conditions. Due to the adjustable control action of the FLC approach depending upon varying system variables, it is widely used for the control of PV-fed multilevel inverter systems [7], [13],[15]. Stonier et al. have carried out the investigation of FLC of solar-PV-fed modular multilevel inverter [7]. Kurian et al. have done the investigation of the MPPT technique of a sustainable PV system using a fuzzy logic controller and its effect on harmonics [13]. Furthermore, Gopinath et al. have done the investigation of interval type-2 fuzzy logic control of a solar integrated cascaded multilevel inverter [15]. In the suggested structure, the battery of the electric vehicle can offer yet another means of storing and exchanging energy. Power is supplied to the battery during the process of charging, while power from the battery can be delivered to either the DC-link or to the grid through the process of discharging. Energy flows in both directions are controlled by a bidirectional DC-DC converter [10]. The structure of converters used in PV-integrated EV charging and bidirectional power flow can be found in [9]. Grid connection of PV and battery systems utilizing a modular multilevel isolated SEPIC converter has been considered in [10], while the design of a multilevel boost inverter for renewable energy systems and electric vehicles has been described in [11]. Harmonic performance is another parameter that needs consideration when nonlinear loads are connected to the power grid since these loads are capable of producing harmonic currents in the electrical system [8], [13], [14]. FLC-based MPPT performance analysis in terms of harmonic reduction in a PV system was performed in [13], whereas grid current quality in PV-interfaced cascaded H-bridge nine-level inverters was analyzed in [8]. Multilevel inverter topologies, control and PWM techniques for grid-connected PV systems were described in [14]. The above literature studies form the foundation for performance analysis of the harmonic characteristics of the proposed system. Filter-assisted harmonic mitigation of a grid-connected nine-level inverter will be considered in the current research work.

In this regard, the system considered in the current research work consists of solar PV generation, a nine-level inverter, an EV lithium-ion battery storage, utility grid connection and nonlinear load compensation. A TOSSI-based fuzzy logic controller will be employed to control the inverter under varying PV generation and battery conditions. Analysis of the proposed system will be conducted for various PV generation power, battery charge/discharge operations, grid current THD and power flow behavior.

III. PROPOSED SYSTEM MODELLING

Fig. 1, illustrates a proposed model of a grid-connected PV–EV system comprising a solar PV array, MPPT-controlled boost converter, nine-level inverter, EV lithium-ion battery, bidirectional DC-DC converter, nonlinear load, filter, and utility grid [9]. The system is developed in MATLAB/Simulink to study power flow, battery operation, inverter response, and grid-current quality under different conditions.

The PV array supplies power through the MPPT and boost converter to maintain the required DC-link voltage. The connection between the EV battery and the system is done using a two-way DC-DC converter, which charges/discharges depending on the PV power available in the system [9], [10]. The nine-level inverter converts the DC-link power to AC for the grid and load, while the filter reduces switching harmonics and supports compensation of nonlinear-load currents.

Control of the inverter is done through a TOSSI-based fuzzy logic controller. TOSSI provides the sinusoidal reference, and the FLC uses the error and change in error to generate the control signal for PWM switching. The system is tested under different PV power levels and battery operating modes, with PV/battery power, SOC, inverter voltage, grid power, and grid-current THD considered for performance evaluation.

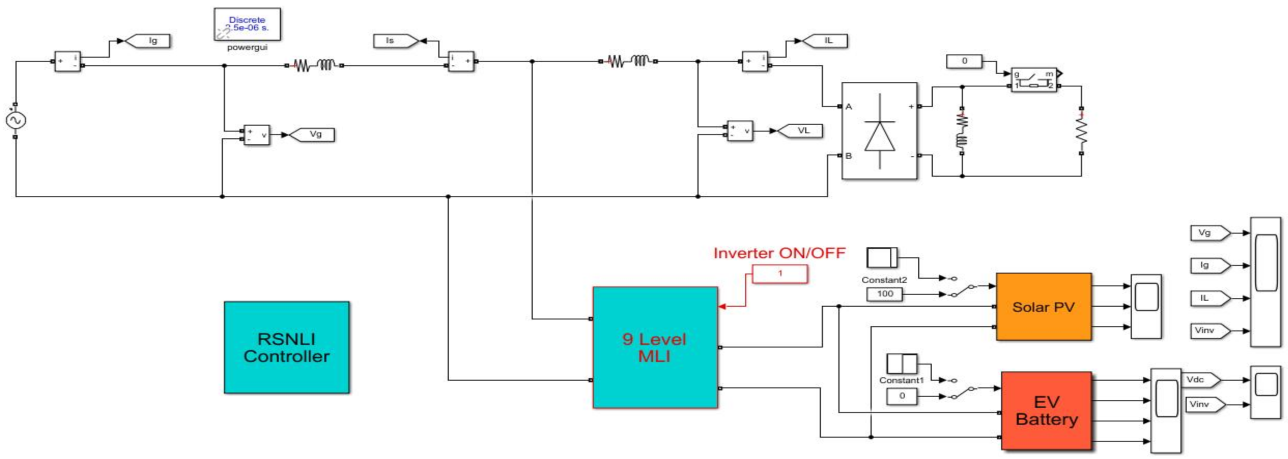

Fig. 1 Proposed configuration of nine-level inverter integrating PV and EV battery systems

A. Parameters of system configuration

Table 1: Parameters of PV and EV systems

Parameter	Symbol	Value
Solar PV specifications		
Cells per module	N	60 cells
Parallel Strings	-	3
Series-Connected modules per string	-	8
Maximum Power	W	213.15 W
Open circuit Voltage	V_{oc}	36.3 V
Short Circuit Current	I_{sc}	7.84 A
Voltage at Maximum Power Point	V_{mp}	29 V
Current at maximum power point	I_{mp}	7.35 A
Temperature coefficient	V_{oc}	-0.36 deg.c
Temperature coefficient	I_{sc}	0.10 deg.c
EV battery (Lithium-Ion) specifications		
Nominal Voltage	V	200 V
Rated Capacity	Ah	240 Ah
Initial State of charge	%	80 %
Battery Response Time	Sec	1 Sec
Maximum capacity	Ah	240 Ah
Cut-off voltage	V	150 V
Fully charged Voltage	V	232.7 V
Nominal discharge current	A	104.3 A
Capacity at nominal voltage	Ah	217.04 Ah

B. Nine-level inverter

As shown in Fig. 2, the inverter is powered from the positive and negative terminals of the DC link [2], [3], [4], [12], [14]. Four capacitors are arranged in series across the link so that the total DC voltage is distributed among four sections. The individual capacitor voltages are measured as V_{dc1}, V_{dc2}, V_{dc3}, and V_{dc4}, while the complete DC-link voltage is denoted by V_{dc} [4], [14]. These voltage measurements are continuously provided to the control system to observe the DC-link operating condition and keep the capacitor voltages properly balanced. In addition, an inverter enable signal is used to start or stop the inverter according to the required operating condition.

Voltage across DC is:

$$V_{dc}=V_{dc1}+V_{dc2}+V_{dc3}+V_{dc4} \quad (1)$$

The inverter's switching stage contains six switches, S1 through S6, and these switches decide how the DC link voltage is sent to the output. Each switching state connects capacitor sections to the circuit, and this lets the inverter build the voltage level. The diodes give paths for the current to flow and keep the DC- link sections separated while the inverter works.

Because of this, the inverter creates a stepped output waveform [4], [14] that has voltage levels, and it does so without using a huge number of semiconductor switches. The selected voltage is then supplied to the H-bridge formed by switches S_7, S_8, S_9, and S_{10}. The polarity of the voltage from the inverter is determined by the H-bridge. By changing the switching combination, the same voltage can be applied in either direction, allowing the inverter to generate both positive and negative output voltage levels.

With four voltage steps on either side of the zero level, the inverter generates the following nine output levels $+4V_{dc}, +3V_{dc}, +2V_{dc}, +V_{dc}, 0, -V_{dc}, -2V_{dc}, -3V_{dc}, -4V_{dc}$, through which the level-selection circuit selects the voltage magnitude [2], [3], [12].

The inverter also acts as an active filter that injects reactive power into the circuit to cancel the harmonics generated. The filter helps smooth the stepped inverter waveform generated at nine voltage levels, which is near a sinusoidal waveform.

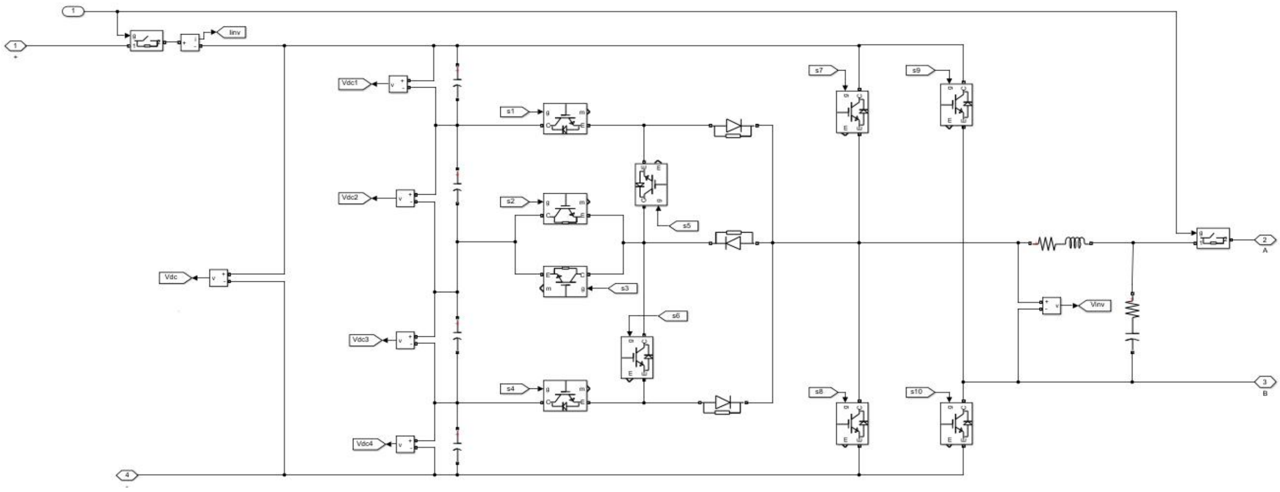

Fig. 2 Topology of a nine-level inverter with DC link and filter

C. Fuzzy Logic Controller

A TOSSI (Third-Order Sinusoidal Signal Integrator) is used to obtain a suitable sinusoidal reference from the measured electrical waveform. The generated reference was compared with the corresponding measured system quantity to determine the error and its change. These error signals were supplied to the fuzzy logic controller as shown in Fig.2, which evaluated them using predefined fuzzy rules and generated the required control signal. The controller output was then applied to the modulation stage to generate suitable gate pulses for the nine-level inverter using a PWM inverter [7], [15]. Therefore, TOSSI supports accurate reference generation, while the FLC helps the inverter maintain proper performance under changes in solar PV power, grid conditions, and EV charging demand.

In the current model of fuzzy control algorithm, the number of rules is 25. The two input signals are characterized by five linguistic values: Negative Big (NB), Negative Small (NS), Zero (Z), Positive Small (PS), and Positive Big (PB). The actual input values are first translated into linguistic terms by means of fuzzification, and the rules are then evaluated through Mamdani inference procedure.

Every rule is fired based on the membership value of their input variables, which is generally determined using the minimum or multiplication method. After that, the results of all the fired rules in the form of fuzzy outputs are aggregated, generally using the maximum method.

Defuzzification involves taking the output fuzzy set after the inference process and turning it into a crisp value. The resulting crisp value will be employed by the controller for deciding on the required action. Based on what the system needs, this signal can change the duty cycle, adjust the modulation index, or create the right reference current. In this way, the fuzzy controller provides the required control response for the power electronic converter under varying operating conditions.

D. Solar PV system

Fig. 3 shows the photovoltaic solar panel array, MPPT, and boost converter. The PV array is the source of renewable energy used in the proposed system. Because the power generated from the PV array is dependent on the irradiation of the sun and its temperature, an MPPT control system was applied for the purpose of following the operating point and obtaining maximum power from the PV system [9], [13]. The MPPT controller continuously monitors the PV voltage and current and generates a suitable duty-ratio command for the boost converter.

The boost converter acts as an interface between the PV array and DC link [9], increasing the variable PV voltage to the level required by the inverter. By adjusting the switching duty ratio according to the MPPT command, the converter maintains the PV array near its maximum power operating point. The extracted solar power is then transferred to the DC-link section for subsequent conversion through the inverter.

The maximum output power is calculated by:

$$\frac{dI_{pv}}{dV_{pv}} = -\frac{I_{pv}}{V_{pv}} \qquad (2)$$

The voltage conversion formula shows the way in which the input voltage is converted into the desired output voltage:

$$V_{dc} = \frac{V_{pv}}{1-D} \qquad (3)$$

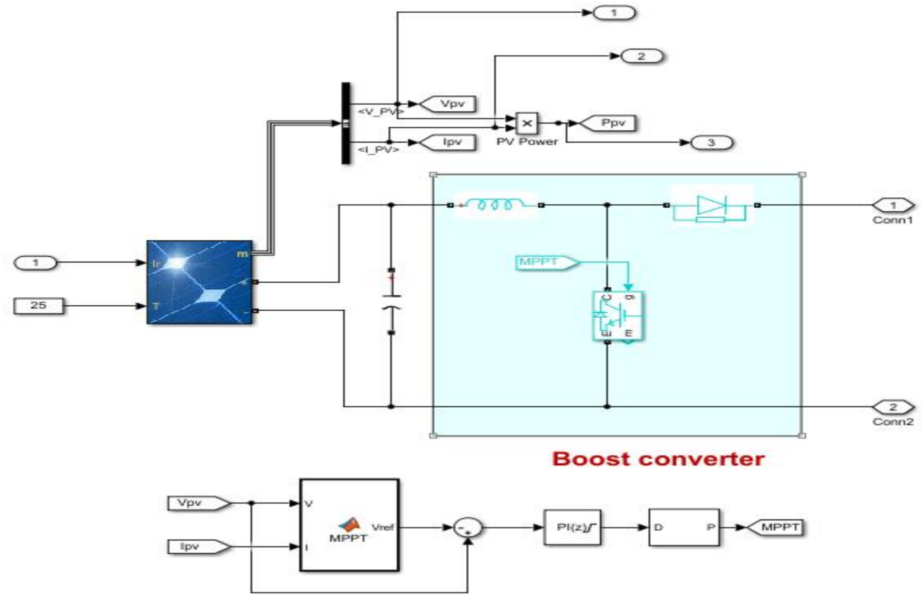

Fig. 3 Solar PV system with MPPT and Boost converter

E. EV battery systems

As shown in Fig.4, the lithium-ion battery will be included in the proposed design in order to serve as an energy storage source for the EV charging station's electricity requirement. If the output power produced by the solar PV system exceeds that required by the load, the extra energy may be stored in the battery. This energy can be released back into the system whenever there is low generation of energy from the solar panels. The reason for using a bidirectional DC-DC converter in the process is that the battery voltage and current change while charging and discharging [9], [10].

The current available for charging the battery can be determined by

$$P_{bat} = V_{bat} \times I_{bat} \qquad (4)$$

where P_{bat} is the battery charging power, V_{bat} is the battery voltage, and $I_{bat}$is the battery charging current.

The SOC is dependent on the rate of charge current. This can be expressed mathematically using the SOC given below.

$$SOC(t) = SOC(t_0) + \frac{1}{Q_{bat}} \int_{t_0}^{t} I_{bat}(\tau)\, d\tau \qquad (5)$$

where $Q_{bat}$is the battery capacity in ampere-hours. Thus, when the charging current remains approximately constant, the battery SOC increases progressively with time.

The energy needed for the battery to charge can also be obtained from

$$E_{bat} = \int P_{bat}(t)\, dt \qquad (6)$$

For approximately constant voltage and current

$$E_{bat} \approx V_{bat} \quad I_{bat} \qquad (7)$$

The battery-side converter is controlled through the use of a proportional-integral (PI) controller to regulate the current during both charging and discharging processes. The error current is defined through comparison between the reference battery current and the battery current is given by

$$e(t) = I_{ref}(t) - I_{bat} \qquad (8)$$

The PI controller processes this error according to

$$e(t)\ u(t) = K_p e(t) + K_i \int e(t)\, dt \quad (9)$$

proportional gain and integral gain of the PI controller are K_p and K_i. The resultant output signal from the controller will be used to produce the switching pulses for the bidirectional DC-DC converter.

As a result, the battery current can be regulated based on the needed operating condition, which lets the lithium- ion battery charge and discharge smoothly and under control.

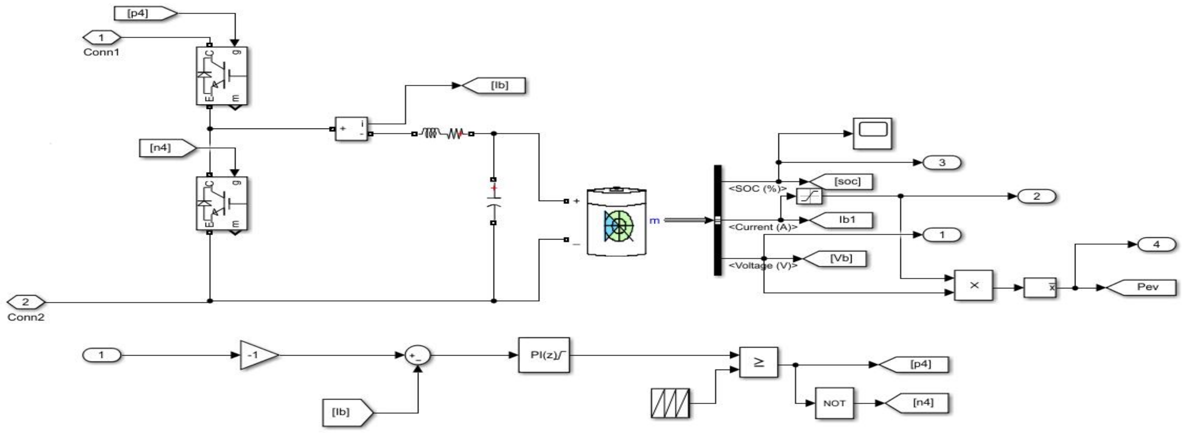

Fig.4 Battery charging system for electric vehicle using PI controller

IV. RESULTS AND DISCUSSION

A. Comparison of THD values

Fig. 5 and Fig. 6 represent THD values of grid current with a non-linear load with the active power filter in switched-on and switched-off positions, respectively. Before connecting the filter, the THD value is 6.64% because of the presence of harmonics in it, but after connecting the filter, the harmonics in the current decrease and the THD value is reduced to 1.14%. The smaller the THD, the better the quality of the grid current as well as the performance of the converter [8], [14].

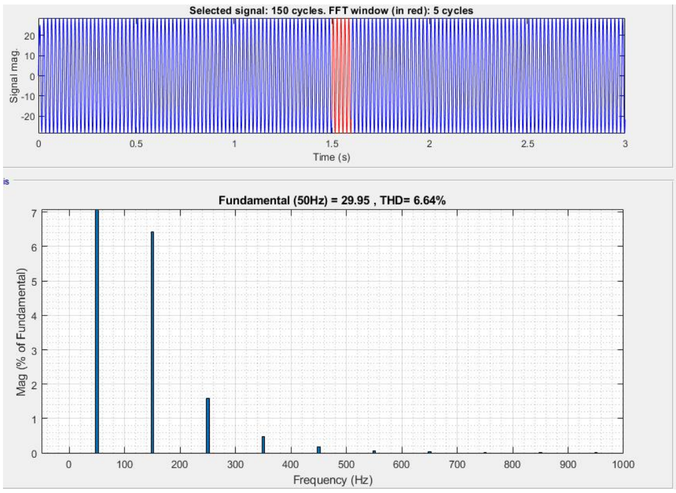

Fig.5 THD value before connecting the filter

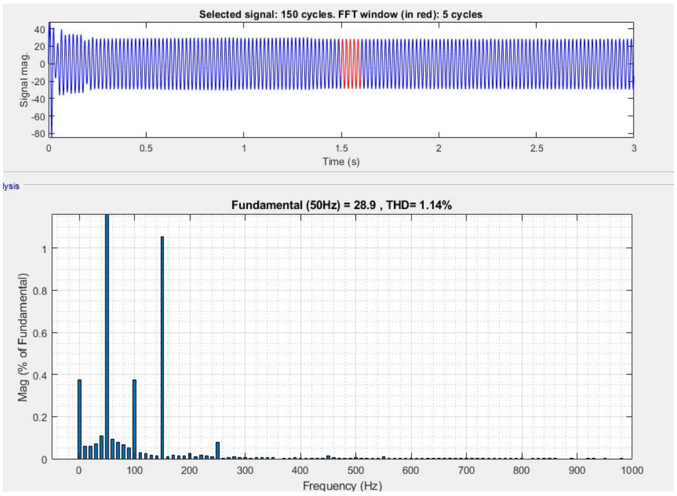

Fig.6 THD value after connecting the filter

B. THD comparison between PI controller and fuzzy logic controller

Both PI and fuzzy logic controllers are used for evaluating the performance of the system under identical operating conditions, as shown in Table 2. To be precise, the five-level inverter shows a THD value of 3.60% for grid current, but the nine-level inverter with a PI controller shows 1.42% THD after the filter connection. On the other hand, the nine-level inverter with an FLC controller reduces the THD value to 1.14%. The reason behind choosing the fuzzy logic controller is the adaptation of the control action according to the error and its time derivative, because the PI controller works with constant control gain. Thus, the fuzzy logic controller will provide the ability to work efficiently under changing conditions such as PV power generation, EV battery charging, discharging, and nonlinear loads.

Table 2: Comparison table for PI and Fuzzy logic controllers

S.NO	Filter(on/off)	MLI used	Controller used	THD Values
1	off	Five level	PI controller	27.38
2	On	Five level	PI controller	3.60
3	Off	Nine level	PI controller	10.69
4	On	Nine level	PI controller	1.42
5	Off	Nine level	Fuzzy Logic Controller	6.64
6	on	Nine level	Fuzzy Logic Controller	1.14

C. Battery in charging condition

1. Solar irradiance at 1000w/m^2: At an irradiance of 1000 W/m² (as shown in Fig.7), the solar PV array produces its rated power and operates near the maximum power point. During battery charging, the PV system supplies power to the connected load, and the remaining available power is directed to the EV battery [9], [10]. It will assist in reducing the consumption of energy from the utility grid. Since there is no loading of power during this time, the amount of power produced by the solar panel system is fed into the battery storage. Thus, the amount of power flow to the grid utility system is minimized.

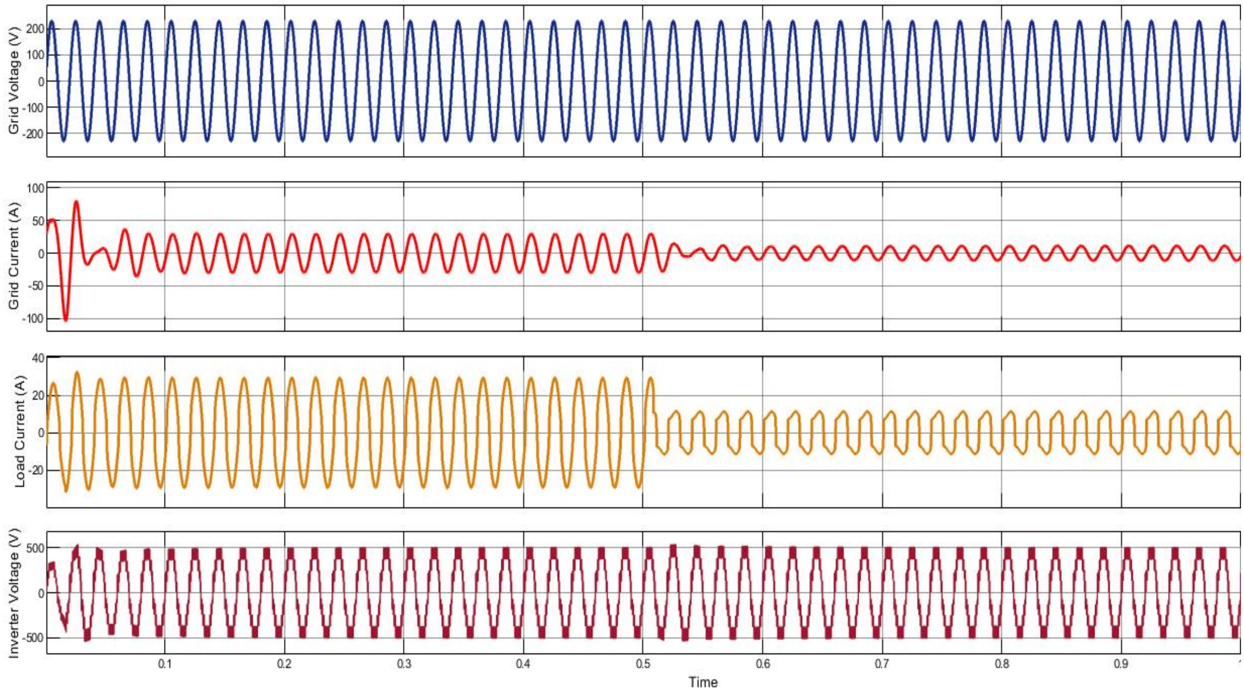

Fig. 7 Dynamic performance of battery at PV 1000w/m^2. The load is removed at 0.5 sec.

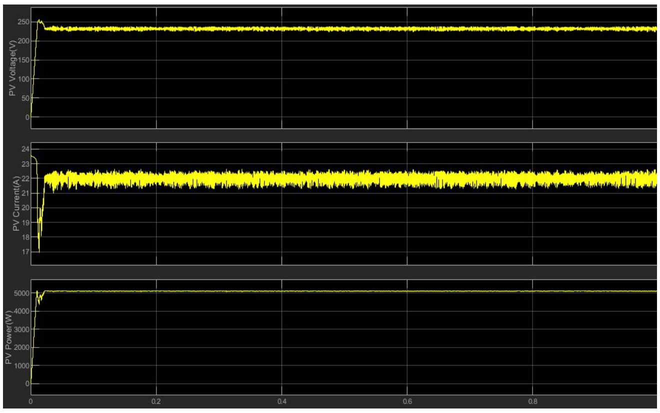

Fig.8 PV voltage, current, power response at 1000w/m^2 irradiation

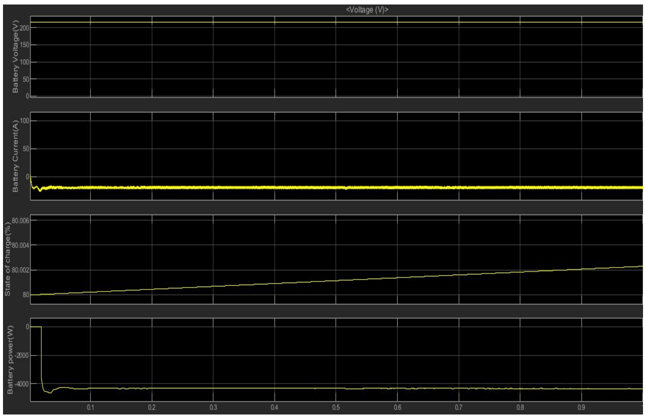

Fig.9 EV battery voltage, current, soc, power response at 1000w/m^2 irradiation

The simulation (Fig.8 and Fig.9) shows the charge of the battery of the EV with the power produced from the PV module. Since the irradiation level and temperature are constant, the output power from the PV is steady at 230V and 22A, meaning the power produced is approximately 5kW. There are small fluctuations of both voltage and current levels because of the switching action and MPPT algorithm. During the charging process, the battery runs at 215V and 20A, receiving almost 4.3kW, while increasing the SOC of the battery. There is a small transient at the beginning due to the steady-state of the converter and controller.

2. Solar irradiance at 500w/m^2: At an irradiance of 500 W/m², as shown in Fig.10, the solar PV array produces its rated power and operates near the maximum power point. During battery charging, the PV system supplies power to the connected load, while the remaining available power is directed to the EV battery. It will assist in reducing the consumption of energy from the utility grid. Since there is no loading of power during this time, the amount of power produced by the solar panel system is fed into the battery storage. Thus, the amount of power flow to the grid utility system is minimized.

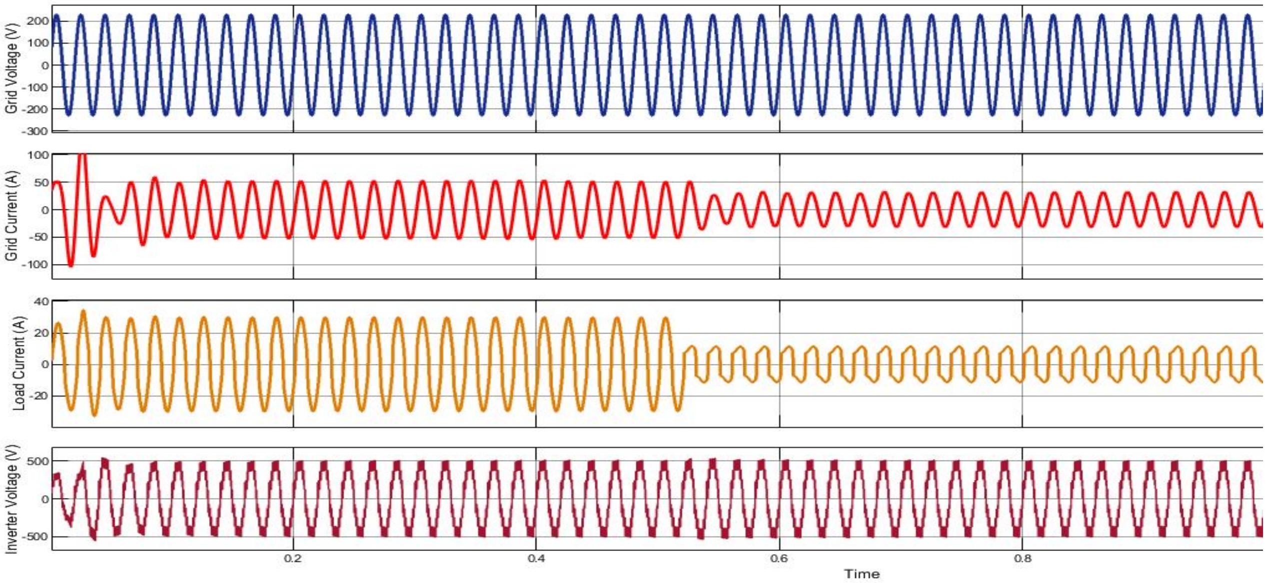

Fig.10 Dynamic performance of the battery at PV 500w/m^2. The load is removed at 0.53 sec.

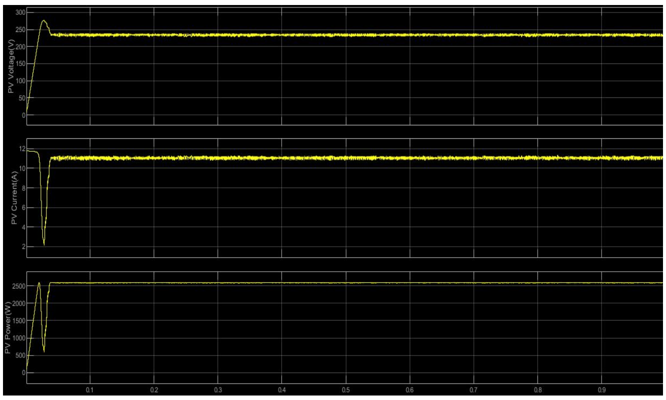
Fig.11 PV voltage, current, power response at 500w/m^2

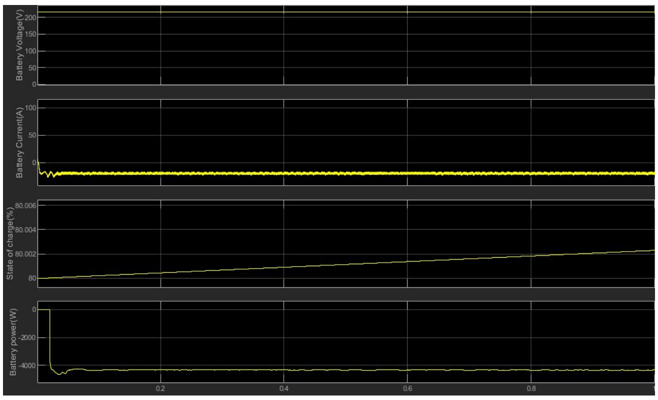
Fig. 12 Ev battery voltage, current, soc, power response at 500w/m^2 irradiation

As shown in Fig.11 and Fig.12, during the initial operation, the MPPT controller shows a short transient before reaching the maximum power point at around 233 V, 11 A, and 2.6 kW within 0.04 s. Once settled, the PV output remains nearly constant with only small ripples under constant irradiance and temperature. The EV battery is charged at approximately −20 A, corresponding to a charging power of about −4.3 kW, with a brief overshoot to nearly −4.6 kW during the first 0.05 s. The battery SOC increases from 80% to about 80.0025% over 1 s, while the small current fluctuations are mainly due to converter switching.

D. Battery in Discharging condition

1. Solar irradiance at 1000w/m^2: At an irradiance of 1000 W/m² (as shown in Fig.13), the PV array operated close to its maximum power point and delivered a high amount of power. During battery discharging, the PV system supplies power to the connected load, and the EV battery provides the additional power required to meet the demand. Once the load is removed, the power available from the PV source is utilized within the system, and the battery can transfer its stored energy to the grid. The increase in grid power supply results in an increase in grid current.

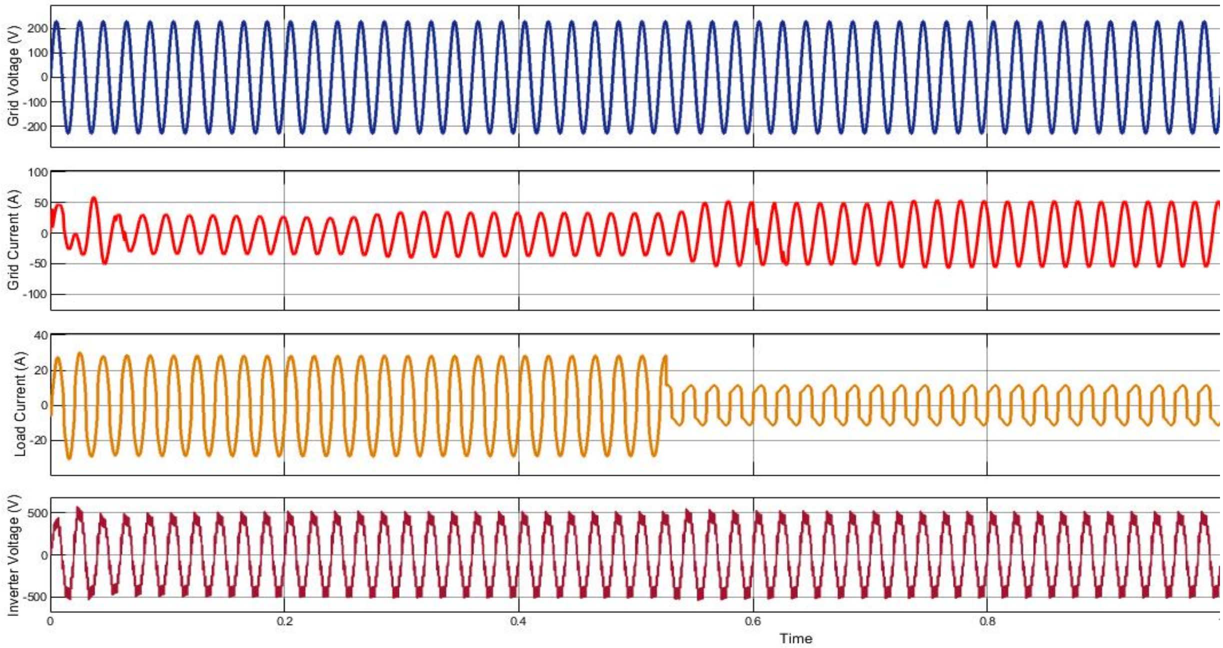

Fig.13 Dynamic performance of battery at PV 1000w/m^2. The load is removed at 0.52 sec.

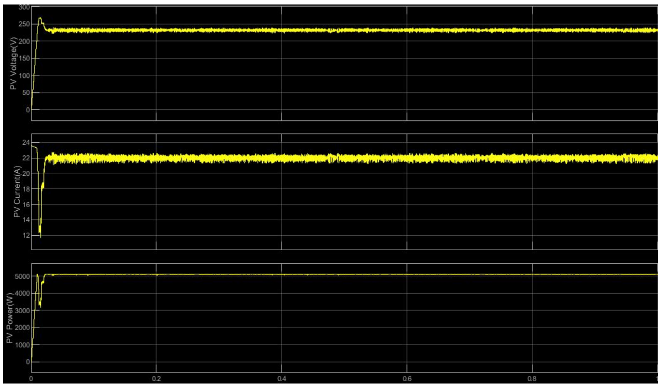

Fig.14 PV voltage, current, power response at 1000w/m^2 irradiation

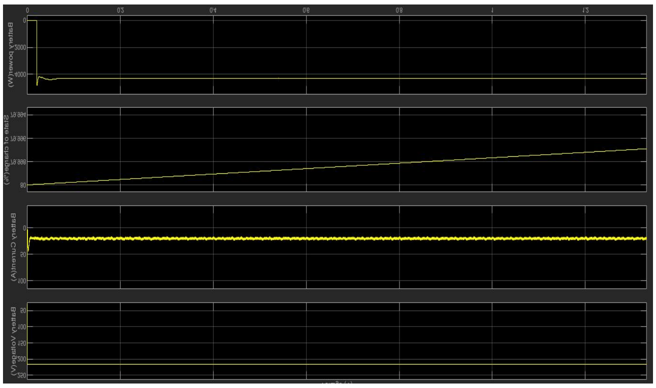

Fig.15 Ev battery voltage, current, soc, power response at 1000w/m^2 irradiation

These simulation results (as illustrated in Fig.14 and Fig.15) reveal the behavior of the PV-EV battery system within the time span of one second of its operation. At the beginning, the PV voltage rises to nearly 265 V within 0.02 s, while the current changes from about 23.5 A to 12 A as the controller establishes the operating point. It then settles around 230 V and 22 A, producing approximately 5.1 kW, with only small switching-related ripples. On the battery side, the voltage remains close to 215 V, while the current has an initial peak of about 45 A before settling near 20 A. The SOC changes slightly from 80% to 79.997% during the simulation. The decrease in SOC indicates battery discharging according to the Simulink sign convention.

2. Solar irradiance at 500w/m^2:

At an irradiance of 500 W/m² (as shown in Fig.16), the PV array operated close to its maximum power point and delivered a high amount of power. During battery discharging, the PV system supplies the connected load, and the EV battery provides the additional power required to meet the demand.

Once the load is removed, the power available from the PV source is utilized within the system, and the battery can transfer its stored energy to the grid. The increase in grid power supply results in an increase in grid current.

The simulation (as shown in Fig.17 and Fig.18) shows the PV and EV battery response under reduced solar power for a duration of 1 s. At the start, the PV voltage increases to about 275 V within 0.04 s, while the current falls from nearly 11.8 A to 2 A as the controller settles at the operating point. The PV output then becomes steady at around 233 V and 11 A, giving approximately 2.55 kW of power with small switching-related ripples. The battery voltage remains nearly constant at 215 V, while its current initially peaks at about 45 A and then settles close to 20 A. The battery supplies approximately 4.3 kW, causing its SOC to decrease slightly from 80% to 79.9977%. Since the available PV power is lower than the battery power demand, the battery provides the additional power required by the system, corresponding to discharge operation.

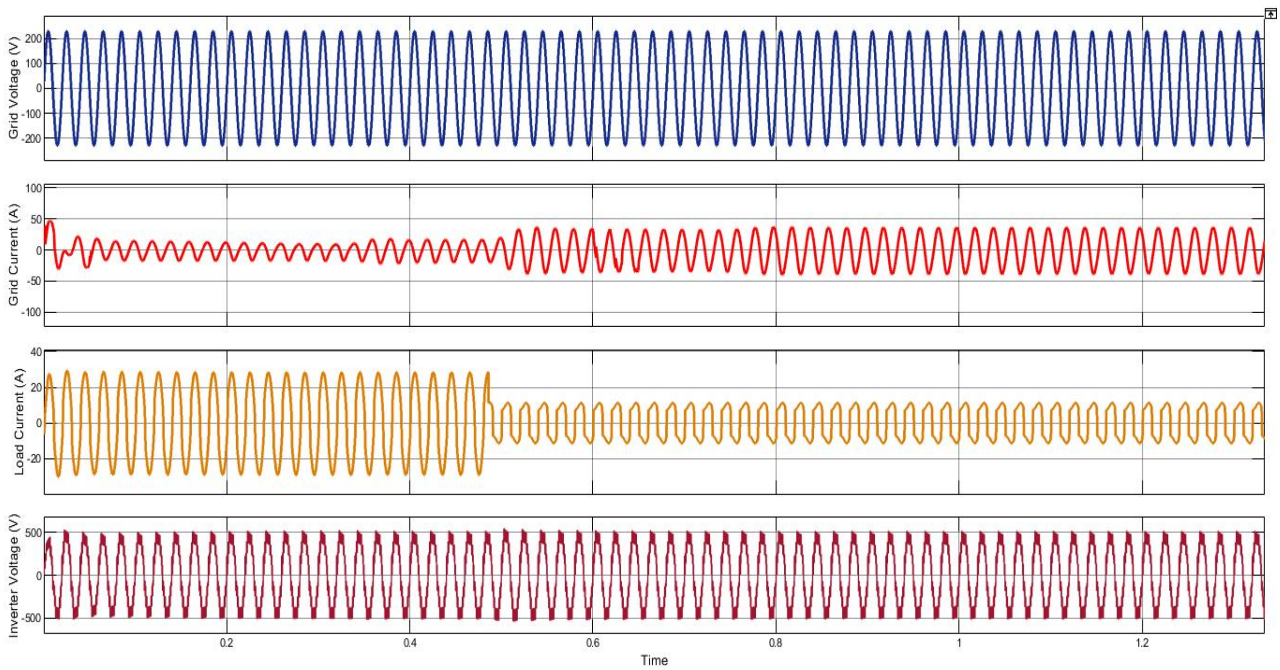

Fig.16 Dynamic performance of battery at PV 500w/m^2. The load is removed at 0.5 sec.

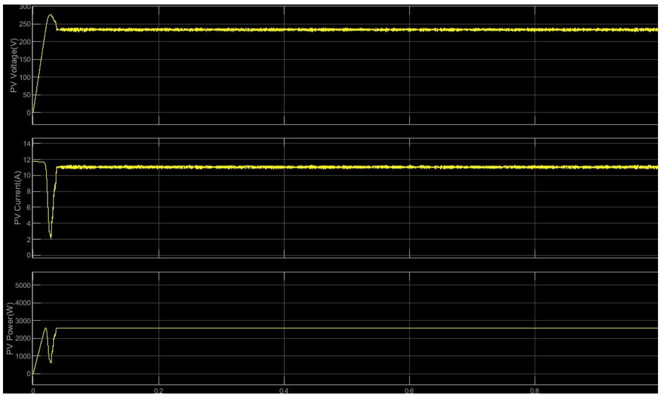

Fig.17 PV voltage, current, power response at 500w/m^2

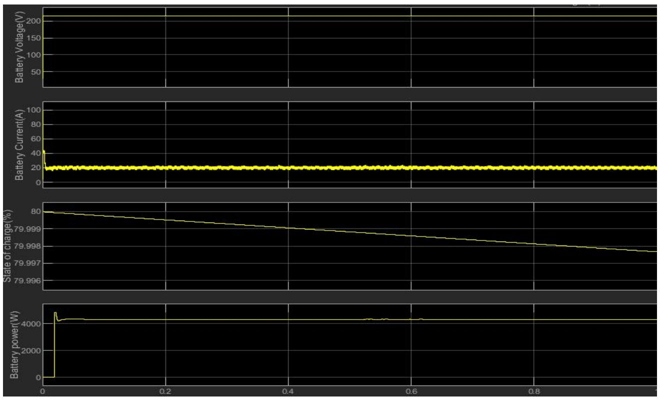

Fig.18 Ev battery voltage, current, soc, power response at 500w/m^2 irradiation

V. CONCLUSION

The proposed system was tested in simulation with the PV source, EV battery, utility grid, and nonlinear load under different operating conditions. The nine-level inverter produces the required stepped voltage, while the bidirectional DC-DC converter manages the battery during charging and discharging [9], [14]. The FLC adjusts the inverter response based on the power requirements of the PV source, battery, and load. With the filter connected, the grid-current THD is reduced from 6.64% to 1.14%. The results under different irradiance levels also show that power is properly shared between the PV source, battery, grid, and load. Overall, the simulation results confirm stable operation and effective power management with an increase in power quality, reduction of harmonics, while lowering grid dependency and increasing system stability in the proposed system. Further work can investigate the proposed system at higher power levels and with larger PV and EV battery capacities, verify its performance using real-time or hardware-based implementation, and study advanced control methods such as adaptive fuzzy and ANN-based techniques for improved operation during complex charging, discharging, G2V, and V2G conditions.

VI. REFERENCES

[1] S. T. Tan, D. Ishak, R. Mohd-Mokhtar, S. S. Lee, and N. R. N. Idris, “Predictive control of plug-in electric vehicle chargers with photovoltaic integration,” *J. Mod. Power Syst. Clean Energy*, vol. 6, pp. 1264–1276, 2018, doi: 10.1007/s40565-018-0411-7.

[2] M. K. Das, K. C. Jana, and A. Sinha, “Performance evaluation of an asymmetrical reduced switched multi-level inverter for a grid-connected PV system,” *IET Renewable Power Generation*, 2018, doi: 10.1049/iet-rpg.2016.0895.

[3] M. B. Satti, A. Hasan, and M. I. Ahmad, “A new multilevel inverter topology for grid-connected photovoltaic systems,” *Int. J. Photoenergy*, 2018, doi: 10.1155/2018/9704346.

[4] P. M. Bana *et al.*, “Recently developed reduced switch multilevel inverter for renewable energy integration and drives application: Topologies, comprehensive analysis and comparative evaluation,” *IEEE Access*, 2019, doi: 10.1109/ACCESS.2019.2913447.

[5] P. Lingom *et al.*, “Analysis and control of PV cascaded H-bridge multilevel inverter with failed cells and changing meteorological conditions,” *IEEE Trans. Power Electron.*, 2021, doi: 10.1109/TPEL.2020.3009107.

[6] M. J. Sathik, D. J. Almakhles, N. Sandeep, and M. D. Siddique, “Experimental validation of new self-voltage balanced 9L-ANPC inverter for photovoltaic applications,” *Sci. Rep.*, vol. 11, p. 5067, 2021, doi: 10.1038/s41598-021-84531-z.

[7] A. A. A. Stonier *et al.*, “Fuzzy logic control for solar PV fed modular multilevel inverter towards marine water pumping applications,” *IEEE Access*, 2021, doi: 10.1109/ACCESS.2021.3090254.

[8] A. Gupta *et al.*, “Power quality evaluation of photovoltaic grid interfaced cascaded H-bridge nine-level multilevel

inverter systems using D-STATCOM and UPQC," *Energy*, 2022, doi: 10.1016/j.energy.2021.121707.

[9] F. Nasr Esfahani, A. Darwish, and B. W. Williams, "Power converter topologies for grid-tied solar photovoltaic (PV) powered electric vehicles (EVs)—A comprehensive review," *Energies*, vol. 15, no. 13, p. 4648, 2022, doi: 10.3390/en15134648.

[10] F. Nasr Esfahani, A. Darwish, and A. Massoud, "PV/battery grid integration using a modular multilevel isolated SEPIC-based converter," *Energies*, vol. 15, no. 15, p. 5462, 2022, doi: 10.3390/en15155462.

[11] A. Maurya and A. Mishra, "A single source based multilevel boost inverter with reduced peak standing voltage for renewable energy and EV applications," *Renewable Energy Focus*, 2022, doi: 10.1016/j.ref.2022.05.002.

[12] A. A. Al-Samawi and H. Trabelsi, "New nine-level cascade multilevel inverter with a minimum number of switches for PV systems," *Energies*, vol. 15, no. 16, p. 5857, 2022, doi: 10.3390/en15165857.

[13] G. M. Kurian, P. A. Jeyanthy, and D. Devaraj, "FPGA implementation of FLC-MPPT for harmonics reduction in sustainable photovoltaic system," *Sustainable Energy Technol. Assess.*, vol. 52, p. 102192, 2022, doi: 10.1016/j.seta.2022.102192.

[14] P. A. V. Prasad and C. Dhanamjayulu, "An overview on multi-level inverter topologies for grid-tied PV system," *Int. Trans. Electr. Energy Syst.*, 2023, doi: 10.1155/2023/9690344.

[15] B. Gopinath, S. Suresh, and M. Geetha, "Solar integrated cascaded topology of multilevel inverter using interval type-2 fuzzy logic controller," *Electric Power Components and Systems*, 2023, doi: 10.1080/15325008.2023.2210565.